

Cascade Control Solution for Traction Motor for Hybrid Electric Vehicles

Zsuzsa Preitl, Péter Bauer

Department of Control and Transport Automation
Budapest University of Technology and Economics
H-1111 Budapest, Hungary
E-mail: preitl@sch.bme.hu, bauer.peter@mail.bme.hu

József Bokor

Computer and Automation Research Institute
Hungarian Academy of Sciences
H-1518 Budapest, Hungary
E-mail: bokor@sztaki.hu

Abstract: In this paper a hybrid electric vehicle is considered, which contains both an internal combustion engine and an electric motor (EM). Without focusing on the other components of the vehicle, the EM is treated in detail, both regarding modelling aspects and control solutions.

After a brief modelling of the plant, two cascade speed control solutions are presented: first a classical PI+PI cascade control solution is presented. The control systems related to traction electric motors (used in vehicle traction) must be able to cope with different requests, such as variation of the reference signal, load disturbances which depend on the transport conditions and parametric disturbances regarding changes in the total mass of the vehicle. For this purpose, in the design of the speed controller (external loop) a specific methodology based on extension of the symmetrical optimum method is presented. The controllers are developed using the Modulus–Optimum method for the inner loop, and the Extended Symmetrical Optimum Method, corrected based on the 2p-SO-method, for the outer loop (for a more efficient disturbance rejection).

In order to force the behaviour of the system regarding the reference input, a correction term is introduced as a non-homogenous structured PI controller solution.

Simulations were performed using numerical values taken from a real application consisting in a hybrid vehicle prototype, showing satisfactory behaviour.

Keywords: Electric Hybrid Vehicle, Driving system, Speed control, Extended Symmetrical Optimum method, 2p-SO-m

1 Introduction

Electric motors (EM) are used in a large variety of applications in industry, one of them is traction motors. Low power traction motors in electrical drive vehicles are frequently oriented on DC-machines (DC-m) or brushless DC motors (BLDC-m) [3], [4], [5] (but other solutions are also used). From the point of view of mathematical modelling, the two solutions differ only insignificantly, mainly on parameter calculus relations.

The control systems related to traction electric motors (used in vehicle traction) must be able to cope with different requests, determined by the multitude of conditions to which the process must fulfill:

- the vehicle's speed must be adapted to the actual traffic conditions, as a consequence, the *reference of the system* is permanently variable;
- depending of the vehicle velocity, route, weather etc., *load type disturbances* are permanently present and changing;
- with the modification of the total mass of the vehicle the *equivalent moment of inertia* is also modifying, and so the large time constant of the vehicle, resulting in a varying *parametric disturbance*;

These conditionings impose a tuning of the control parameters which fulfil simultaneously all requests. The paper is focused on control solution for an electrical driving application (electrical traction) as part of a hybrid electric vehicle. Details regarding the vehicle itself can be found in [1], [2].

The paper is structured as follows. Section II presents a detailed mathematical model of a separately excited DC-machine. Section III describes two control strategies applied for speed control, both consisting in cascade control. Section IV introduces the numerical values used, and based on these, simulations are performed and analysed. Finally, section V concludes the paper.

2 Plant Model

2.1 General Aspects

The functional block diagram of a series hybrid electric vehicle (HEV) is presented in Figure 1. The main components of the system are: the EM, which drives the wheels and whose control is dealt with in the paper (it can also work as a generator during regenerative braking), the electric generator which delivers electrical energy for the EM, a battery, the controllers and the power electronics. The electric generator is in rigid connection with the internal combustion engine.

2.2 Basic Equations

The operating range of a DC-m is divided into four quadrants: forward motoring, forward braking, reverse motoring and reverse braking [5], [6], [7]. For the driving system (EM and the vehicle) a qualitative and quantitative modelling is used. The mathematical model of the driving system includes both the model of the motor and the dynamical model of the system.

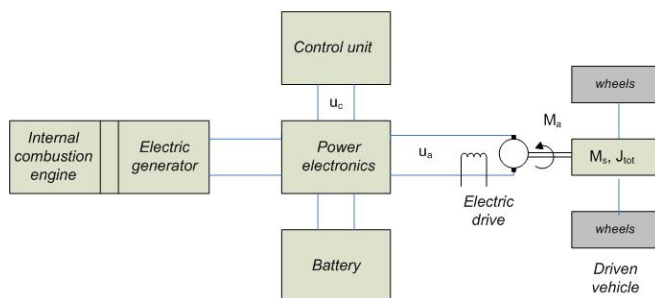


Figure 1

Functional block diagram of a series hybrid electric vehicle

- *Modelling of the motor.* The hypotheses accepted at modelling imply that in normal regimes the DC-m works in the linear domain where the flux (current) is constant in value (valid also for BLDC-m). A change in the excitation regime modifies the basic model, but a linearization in the new working point results in the basic situation.

The basic equations that characterize the functionality of the system are given in (1), where the following notations were used: T_A – time constant of the actuator (power electronics) [sec], u_a – armature voltage [V], k_a – actuator gain, u_c – command voltage from controller [V], L_a – inductance [H], T_a – electrical time constant, i_a – field current [A], e – counter electromotive voltage [V], k_e – coefficient [V/rad/sec], ω – rotor speed [rad/sec], J_{tot} – total moment of inertia of the plant [kgm²], M_a – active torque [Nm], M_s – load torque [Nm], M_f – friction torque [Nm], J_m – moment of inertia of the DC-m [kgm²], J_{veh} – moment of inertia of the vehicle reduced to the motor axis [Nm²], J_w – moment of inertia of the two driven wheels reduced to motor axe (converted) [kgm²].

$$\begin{aligned}
 T_A \cdot \dot{i}_a + u_a + k_a &= u_c \\
 L_a \cdot \dot{d}i_a + R_a \cdot i_a &= u_a - e \\
 T_a &= L_a / R_a \quad , \quad e = k_e \omega \\
 M_a &= k_m \cdot i_a \\
 J_T \dot{\omega} &= M_a - M_s - M_f \\
 J_{tot} &= J_m + J_{veh} + J_w
 \end{aligned}
 \tag{1}$$

As a result, the block diagram of the DC-m is depicted in Figure 2. Based on the bloc diagram from Figure 2, the four transfer functions (t.f.s) according to the DC-m can be defined; $\{H_{\omega,uc}(s), H_{\omega,ms}(s), H_{ia,uc}(s), H_{ia,ms}(s)\}$. The main t.f. regarding to which the controller will be designed is $H_{\omega,uc}(s)$; their expressions can be detailed for two more remarkable cases: $k_f \neq 0$ and the approximation case $k_f = 0$ frequently used in practice, rel. (2)-(5)

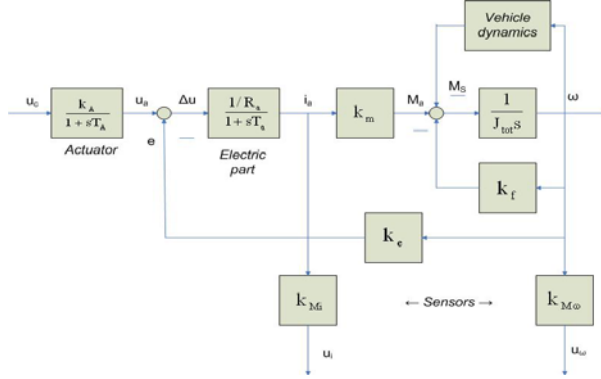


Figure 2
Block diagram of a DC-m

$$H_{\omega,uc}(s) = \frac{k_A}{1 + sT_A} \frac{1/k_e}{1 + sT_m + s^2T_aT_m} \approx \frac{k_A}{1 + sT_A} \frac{1/k_e}{(1 + sT_a)(1 + sT_m)} \quad (2)$$

The factorised for is valid for $T_m \gg T_a$, specific for electric traction.

$$H_{ia,uc}(s) = \frac{k_A}{1 + sT_A} \frac{sT_m/R_a}{1 + sT_m + s^2T_mT_a} \approx \frac{k_A}{1 + sT_A} \frac{sT_m/R_a}{(1 + sT_a)(1 + sT_m)} \quad (3)$$

$$H_{\omega,ms}(s) = -\frac{R_a}{k_mk_e} \frac{1 + sT_a}{1 + sT_m + s^2T_mT_a} \approx -\frac{R_a}{k_mk_e} \frac{1 + sT_a}{(1 + sT_m)(1 + sT_a)} \quad (4)$$

$$H_{ia,ms}(s) = -\frac{R_a}{k_m} \frac{1}{1 + sT_m + s^2T_mT_a} \approx -\frac{R_a}{k_m} \frac{1}{(1 + sT_m)(1 + sT_a)} \quad (5)$$

Where the mechanical time constant is calculated based on relation:

$$T_m = \frac{J_{tot}R_a}{k_mk_e}.$$

The total inertia is calculated as follows. It is supposed, as in eq. (1), that the total inertia contains the inertias of the vehicle, of the DC-m and of the two driven wheels with the drive shaft. This way, from the energy conservation principle, the following are derived:

$$\frac{1}{2} m_{tot} v^2 = \frac{1}{2} J_{veh} \omega^2 \Rightarrow J_{veh} = \frac{m_{tot} v^2}{\omega^2} \quad (6)$$

$$\text{But } \omega = f_r \cdot \omega_v, \quad v = r \cdot \omega_v = r \cdot \frac{\omega}{f_r}$$

$$\text{It results: } J_{veh} = \frac{m_{tot} \cdot r^2 \cdot \omega^2}{f_r^2 \cdot \omega^2} = m_{tot} \frac{r^2}{f_r^2} \quad (7)$$

where: - ω_v - speed of the drive shaft and wheel; - r - radius of the wheel; - m_{tot} - total mass of the vehicle (including the driver); - v - linear velocity of vehicle; - f_r - drive ratio.

• *Equations of the vehicle dynamics.* The basic dynamical equations for the vehicle motion are presented in eq. (6) [1]:

$$\omega(t) = \frac{f_r}{w_r} v(t)$$

$$M_d(t) = \frac{w_r}{f_r} F_d(t) \quad (8)$$

$$F_d(t) = m \cdot \dot{v}(t) + \frac{1}{2} \rho v^2(t) \cdot A_d \cdot C_d + m_{veh} \cdot g \cdot C_r$$

2.3 About Drive Cycles

The testing of the behaviour of a vehicle through simulation requires a given reference that must be followed. Such reference signals, consisting in a pre-defined time-vehicle velocity scheme, are called drive-cycles [1]. In this paper a section of the New European Driving Cycle will be used for testing, consisting in an acceleration, then constant speed, and breaking until zero velocity is reached.

It must also be mentioned that when modelling the electric vehicle a driver behaviour model can also be taken into account, which has effect on the reference delivered to the electric drive. The modelling of the other functional blocks of the electric vehicle is not subject of this paper, but they are described in [1], [2].

3 Control Structures and Controller Design

3.1 Control Aim and Performances

The aims of the control structures applied to the DC-m are grouped as follows:

- To ensure good reference signal tracking (speed) with small settling time and small overshoot (good transients and zero-steady-state error at $v=\text{const.}$ velocity).
- To ensure load disturbance rejection due to modifications in the driving conditions.
- To show reduced sensitivity [8] to changes in the total inertia of the system:

$$J_{tot} = J_{t0} + \Delta J_t \quad \text{with} \quad \Delta J_t \leq 0.25J_{t0} \quad (9)$$

The adopted two solutions are classical ones, both having two control loops in cascade structure:

- One interior control loop of the current, consisting in a PI controller and Anti-Windup-Reset (AWR) measure.
- One external control loop of rotor speed ω [rad/sec] with a PI controller.

The second control structure differs from the first through the outer loop, in which a forcing block was added to correct the current reference for the inner loop. It can decrease the response time of the system.

3.2 Presentation of the Control Loops. Controller Design

The block diagrams of the two control structures are depicted in Figures 3 and 4, in the form of Simulink diagrams. The two controllers, the current controller and the speed controller, are designed separately.

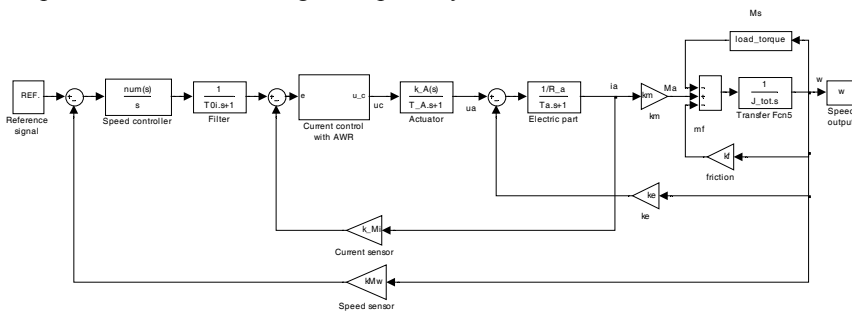


Figure 3

First cascade control structure for the DC-m

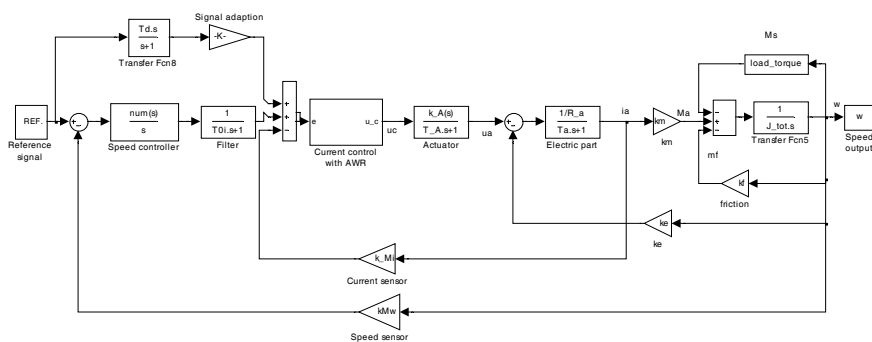


Figure 4

Second cascade control structure for the DC-m

- *The inner current loop* is identical in both cases, and it consists of a PI controller with AWR measure [9], [10]. The parameters of the current controller were determined in accordance with the properties of the inner loop, based on the Modulus Optimum criterion (MO) by Kessler [9], having the relations:

$$C(s) = \frac{k_{ri}}{s} (1 + sT_i), \quad k_{ri} = \frac{1}{2k_{pi} \cdot T_{\Sigma i}}, \quad T_{ii} = T_a \quad (10)$$

Where, k_{pi} – gain of the inner part of the plant, containing the actuator, electric circuit and current sensor), T_a – electric time constant, $T_{\Sigma i}$ – equivalent of small time constants, $T_a > T_{\Sigma i}$.

The AWR measure was introduced to attenuate the effects of going into limitation of the controller. Other methods for handling constraints of the control signal are also used, for example a solution where the controller itself is by a dynamic feedback of a static saturation element [11].

- *The speed control loop*, as the outer loop, consists of a PI controller in two variants for implementation: one homogenous variant and one case when a forcing filter for the reference value was introduced. This second variant ensures the possibility of accelerating the vehicle, depending on the power of the driving motor.

$$P(s) = \frac{k_p}{s(1 + sT_{\Sigma})} \quad (11)$$

where T_{Σ} stands for the current loop and parasitic time constants, k_p characterizes the dynamics of the mechanical part of the driving system (J_{tot}) and the speed sensor (k_{Mo}). The transfer function of the PI controller has the transfer function:

$$C(s) = k_c \left(1 + \frac{1}{sT_c} \right) = \frac{k_c}{s} (1 + sT_c) \quad (12)$$

The open loop transfer function (t.f.) results:

$$L(s) = C(s)P(s) = \frac{k_c k_p (1 + sT_c)}{s^2 (1 + sT_\Sigma)} \quad (13)$$

And so the closed loop t.f. is:

$$H_r(s) = \frac{k_c k_p T_c s + k_c k_p}{s^3 T_\Sigma + s^2 + k_c k_p T_c s + k_c k_p} = \frac{b_1 s + b_0}{a_3 s^3 + a_2 s^2 + a_1 s + a_0} \quad (14)$$

with $b_1 = a_1$, $b_0 = a_0$ (due to the double integrator component in the open loop t.f.)

The design of the speed loop is based on an extension of the SO method from Kessler [7], the Extended Symmetrical Optimum method (ESO-m) [14]; the method is based on the following parameterization:

$$\beta^{1/2} a_0 a_2 = a_1^2, \quad \beta^{1/2} a_1 a_3 = a_2^2 \quad (15)$$

Here β is a parameter that is chosen by the developer. A larger value of β ensures less oscillating transients and a bigger phase margin. Consequently, the controller parameters are calculated with the relations:

$$k_{c0} = \frac{1}{\beta^{3/2} k_p T_\Sigma^2}, \quad T_{c0} = \beta T_\Sigma \quad (16)$$

In second stage, taken into account that $k_f > 0$, the type of the load and that the system performance regarding reference tracking are less satisfactory, the results obtained in the first phase are corrected according to the double parameterization of the SO-m, introduced in [15] as 2p-SO-m and the particularity of the plant (inner loop). Designing the controller based on this approach, there can be ensured:

- Use of pre-calculated (crisp) tuning relations;
- The possibility of improving the system's phase margin, reducing its sensitivity and increasing its robustness;
- The possibility of using controllers with homogenous structure or with non-homogenous structure regarded to the inputs.
- The possibility of improving reference signal tracking by using reference filters with parameters that can be easily fixed.
- The possibility of improving reference tracking using adequate reference filters [15] and load disturbance rejection for some specific cases.

For a second order with lag benchmark type model of the plant, the controller tuning relations specific for 2p-SO-m are close to the ESO method, they allow an efficient correction of the controller parameters depending on the plant's time constants T_l , T_Σ (). For this, the correction relations can be used [15]:

$$k_c = \frac{(1+m)^3}{m} T_\Sigma k_{c0}, \text{ and } \alpha_{k_c}^* = \frac{k_c}{k_{c0}} = (1+m)^3 T_1 \quad (17)$$

$$T_c = T_{c0} \frac{\Delta_m(m)}{(1+m)^3} \text{ and } \alpha_{T_c}^* = \frac{T_c}{T_{c0}} = \frac{\Delta_m(m)}{(1+m)^3} \quad (18)$$

For the chosen value of the β parameter, the controller parameters calculated in the first stage with the ESO-m are corrected regarding the relations (17) and (18), where the values of α_{k_c} and α_{T_c} take into account the values of β and $m = T_{\Sigma a} / T_m$, with $T_{\Sigma a}$ - the time constant that characterizes the inner loop (current) and T_m - the mechanical time constant of the plant (see rel. (2)).

4 Case Study. Simulation Results

4.1 Numerical Values of the Plant

Details and numerical data for the considered application (a hybrid solar vehicle) are presented in [2]. Numerical values of the DC-m in the nominal functioning are synthesized in table 1. Further numerical values used (see also [1], [2]):

- Total mass of vehicle, including an 80kg heavy driver: $m_{tot}=1860 \text{ kg}$;
- Frontal area of vehicle: $A_d=2.4 \text{ m}^2$;
- Air drag coefficient: $C_d=0.4$;
- Air density: $\rho=1.225 \text{ kg/m}^3$;
- Rolling resistance coefficient: $C_r=0.015$;
- Wheel radius: $w_r=0.3 \text{ m}$;
- Final drive ratio: $f_r=4.875$.

The resulting time constants and other plant parameters are enumerated below:

- Mechanical time constant: $T_m=5.4 \text{ sec}$;
- Electrical time constant: $T_a=0.1 \text{ sec}$;
- Total inertia: $J_{tot}=8.6^2$;
- Gain and time constant of actuator: $k_A=30, T_A=0.02 \text{ sec}$;
- Gains for current and speed sensors: $k_{M_i}=0.0238, k_{M_\omega}=0.0178$.

Table 1
Numerical values for nominal functioning

Torque	Rotation	Useful power	Voltage	Current	Absorbed Power	Efficiency
[Nm]	[rot/min]	[kw]	[V]	[A]	[kw]	[-]
50,16	1605	8,43	77,6	126	9,78	86,18

The controller parameters are:

- Current controller: $k_{ri}=7$, $T_{ri}=0.1$ (according to equation (8), plus an AWR time constant according to [9] having the value of $T_t=0.005$;
- Speed controller:
 - o For the first case, see eq.(9): $k_c=35.28$, $T_c=1.75$;
 - o For the second case the controller is the same, the feed forward correction term is of form: $C_{ff}(s) = \frac{560s}{s+1}$.

4.2 Simulation Results

The simulation scenarios are the following: the first control structure is simulated, followed by the second cascade structure simulations (comparison of the currents' and dynamics), ended by simulations for the first case regarding sensitivity aspects for a change in the mass of the plant. The reference signal is the same for all three cases, consisting in an acceleration part, a part with constant velocity and a part of deceleration until a stop is reached. The load of the system is taken into account as in [16].

- (a) Simple cascade structure: Figures 6, 7, 8 and 9.
- (b) Cascade structure with correction of the current reference: in this case the differences in the current behaviour are depicted, together with the active power (dashed line – simple cascade structure, solid line – structure with current correction). The differences in the speed dynamics are not significant, the active power differences are proportional with the current, Figures 10 and 11.
- (c) Simple cascade structure with modified load (Figures 12, 13 and 14) (for the first cascade structure): the mass of the vehicle is changed with +25% of it (solid line – original load, dashed line – increased load):

$$m_{veh} = m_{veh0} + \Delta m = 1860 + 0.25 * 1860 = 2332 \text{ kg.}$$

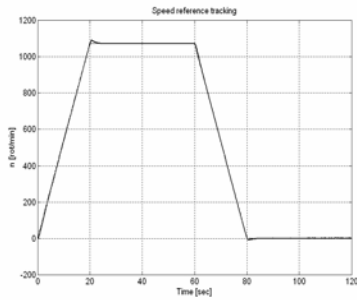


Figure 6
Speed reference tracking

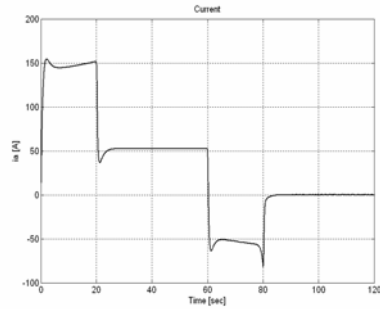


Figure 7
Behaviour of the current

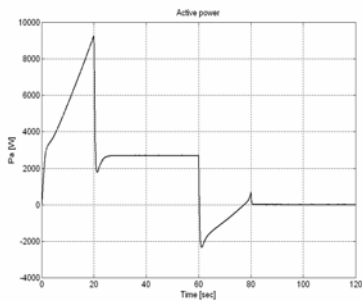


Figure 8
Active power consumption (negative values mean generation)

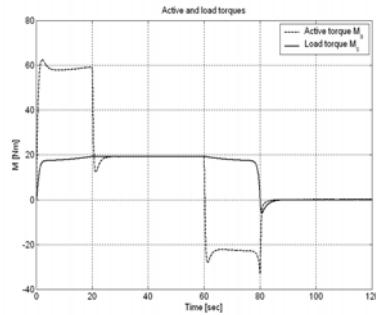


Figure 9
Active torque M_a vs. disturbance torque M_s

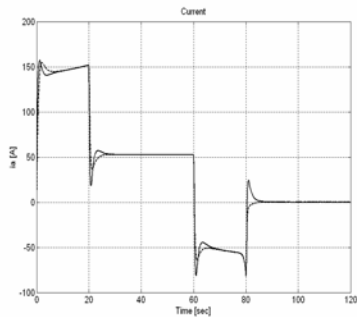


Figure 10
Comparison of the currents

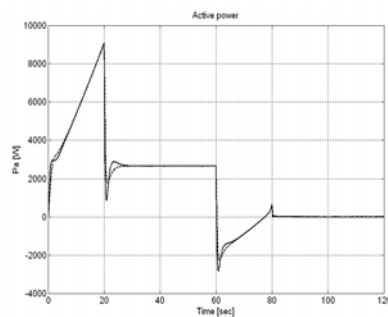


Figure 11
Comparison of the active powers

The speed was not presented since almost the same behaviour resulted. But in order to achieve this performance, the current is higher (since it needs more power to carry the increased weight). Still the current does not reach its maximal

admissible value (4 times the nominal value of 126 A). The active power is higher (12 kW compared to 9 kW at starting), but without exceeding the maximal power of 15 kW of the machine. Both the active torque and the load torque are higher, as expected. Regenerative braking appears when the current (and implicitly the active power) is negative.

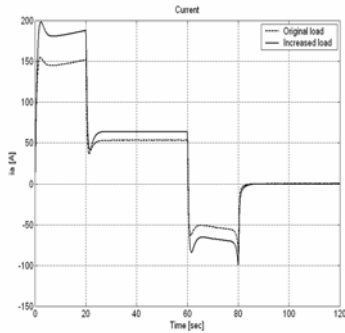


Figure 12
Behaviour of the current

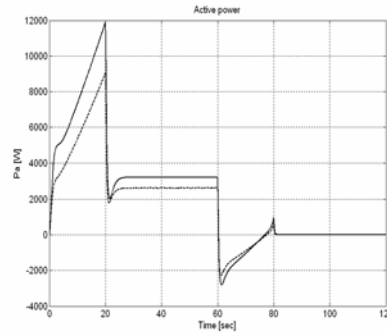


Figure 13
Active power consumption (negative values mean generation)

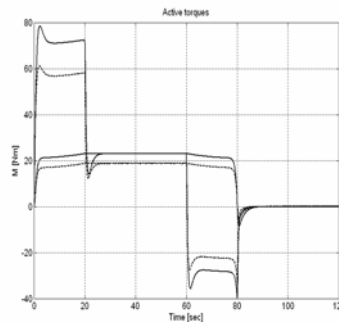


Figure 14
Active torque M_a vs. disturbance torque M_s

Conclusions

The paper presents a cascade control solution for electrical drives used for traction in two variants – without and with a forcing feed forward term for the current reference –, both consisting of cascade control structures. In order to ensure high performances, for controller design different variants of the Modulus Optimum tuning method (MO-m) were used, namely the Extended Symmetrical Optimum method (ESO-m) and a correction of it based on the tuning method named a Double Parameterization of the ESO method (2p-ESO-m), introduced in [15].

Simulations were performed using the Matlab/Simulink environment, for a reference drive cycle. The simulated cases reflect a very good behaviour of the system both regarding reference tracking and also sensitivity to parameter changes. The application considered in the paper is based on a real application of a hybrid solar vehicle.

Acknowledgements

The authors address their thanks to the support from the Hungarian National Office for Research and Technology through the project 'Advanced Vehicles and Vehicle Control Knowledge Center' (ref. number NKTH RET04/2004), which is gratefully acknowledged. The authors also gratefully acknowledge the contribution of Hungarian National Science Foundation (OTKA #K60767).

References

- [1] P. Bauer, Zs. Preitl, T. Péter, P. Gáspár, Z. Szabó, J. Bokor (2006). Control-oriented Modelling of a Series Hybrid Solar Vehicle, *Workshop on Hybrid Solar Vehicles*, November 6, 2006, University of Salerno, Italy
- [1] I. Arsie, R. Di Martino, G. Rizzo, M. Sorrentino (2006). A Model for a Hybrid Solar Vehicle Prototype, *Workshop on Hybrid Solar Vehicles*, November 6, 2006, University of Salerno, Italy
- [2] R. M. Crowder (1998). *Electric Drives and their Controls*, Oxford University Press Inc., New York
- [3] M. Ehsani, K. M. Rahman, M. D. Bellar, A. J. Severinsky (2001). Evaluation of Soft Switching for EV and HEV Motor Drives, *IEEE Transactions on Industrial Electronics*, Vol. 48, No. 1, February 2001, pp. 82-90
- [4] R. Schonfeld (1988). *Digitale Regelung Elektrischer Antriebe*, Dr. Alfred Huthig Verlag, Heidelberg, 1988
- [5] G. Rizzoni (1993). *Principles and Applications of Electrical Engineering*, Richard D. Irwin Inc.
- [6] C.-M. Ong (1998). *Dynamic Simulation of Electric Machinery Using Matlab/Simulink*, Prentice Hall PTR, Upper Saddle River, New Jersey 07458
- [7] K. J. Åström. *Model Uncertainty and Robust Control. Chapter on Control Theory*, (Internet presentation), pp. 63-100
- [8] K. J. Åström, T. Hägglund (1995). *PID Controllers. Theory, Design and Tuning* Research Triangle Park, North Carolina
- [9] P. Hippe, C. Wurmthaler (1999). Systematic Closed Loop Design in the Presence of Input Saturation, *Automatica*, Vol. 40, pp. 1221-1228

- [10] A. Barta, R. Bars, I. Vajk, Zs. Preitl (2005), Practical Controller Design Considering Input Saturation, *6th International Carpathian Control Conference ICCO 2005*, Lillafüred, Hungary, May 24-27, 2005, Proceedings, Vol. I, pp. 51-56
- [11] J. Quevedo, T. Escobet (Editors) (2000). *IFAC workshop on Digital Control. Past present and Future of PID Control, PID'00*, Preprints, Terrassa, Spain, April 5-7, 2000
- [12] K. J. Åström, T. Häggglund (2000). Benchmark Systems for PID Control, *IFAC workshop on Digital Control*, Terrassa, Spain, April 5-7, 2000, pp. 181-182
- [13] S. Preitl, R.-E. Precup (1999). An Extension of Tuning Relations after Symmetrical Optimum Method for PI and PID Controllers, *Automatica*, Vol. 35, No. 10, pp. 1731-1736
- [14] Zs. Preitl (2005). Improving Disturbance Rejection by Means of a Double Parameterization of the Symmetrical Optimum Method, *Scientific Bulletin of the "Politehnica" University of Timișoara, Series Automation and Computers*, Politehnica Publishing House, Timișoara, ISSN 1224-600X, Vol. 50(64), pp. 25-34
- [15] M. Imecs (2000). How to Correlate the Mechanical Load Characteristics, PWM and Field-Orientation Methods in Vector Control Systems of AC Drives, *Buletinul Institutului Politehnic Iasi*, Tomul XLVI (L), Fasc. 5, Electrotehnica, Energetica, Electronica, A X-a Conferința Națională de Actionari Electrice